EINDHOVEN UNIVERSITY OF TECHNOLOGY

Analytical force, stiffness, and resonance frequency calculations of a magnetic vibration isolator for a micro balance

Citation for published version (APA):
Casteren, van, D. T. E. H., Paulides, J. J. H., Janssen, J. L. G., & Lomonova, E. A. (2015). Analytical force, stiffness, and resonance frequency calculations of a magnetic vibration isolator for a micro balance. *IEEE Transactions on Industry Applications*, *51*(1), 204-210. https://doi.org/10.1109/TIA.2014.2328780

DOI:
10.1109/TIA.2014.2328780

Document status and date:
Published: 01/01/2015

Document Version:
Publisher's PDF, also known as Version of Record (includes final page, issue and volume numbers)

Please check the document version of this publication:

• A submitted manuscript is the version of the article upon submission and before peer-review. There can be important differences between the submitted version and the official published version of record. People interested in the research are advised to contact the author for the final version of the publication, or visit the DOI to the publisher's website.
• The final author version and the galley proof are versions of the publication after peer review.
• The final published version features the final layout of the paper including the volume, issue and page numbers.

Link to publication

General rights
Copyright and moral rights for the publications made accessible in the public portal are retained by the authors and/or other copyright owners and it is a condition of accessing publications that users recognise and abide by the legal requirements associated with these rights.

• Users may download and print one copy of any publication from the public portal for the purpose of private study or research.
• You may not further distribute the material or use it for any profit-making activity or commercial gain
• You may freely distribute the URL identifying the publication in the public portal.

If the publication is distributed under the terms of Article 25fa of the Dutch Copyright Act, indicated by the "Taverne" license above, please follow below link for the End User Agreement:

www.tue.nl/taverne

Take down policy
If you believe that this document breaches copyright please contact us at:

openaccess@tue.nl

providing details and we will investigate your claim.

Download date: 04. Oct. 2023

Analytical Force, Stiffness, and Resonance Frequency Calculations of a Magnetic Vibration Isolator for a Microbalance

Dave T. E. H. van Casteren, *Student Member, IEEE*, J. J. H. Paulides, *Senior Member, IEEE*, J. L. G. Janssen, and E. A. Lomonova, *Senior Member, IEEE*

***Abstract*—The accuracy of a microbalance is highly dependent on the level of floor vibrations. One strategy to reduce floor vibrations is a magnetic vibration isolator. Magnetic vibration isolators have the possibility to obtain a zero-stiffness region, which is beneficial for attenuating vibrations. In this paper, a 3-D analytical magnetic surface charge model is used to calculate the spring characteristics of a cone-shaped magnetic vibration isolator for different angles.**

***Index Terms*—Cone shaped, magnetic force, permanent magnets, vibration isolation.**

I. Introduction

In laboratories, weighing is one of the most common tasks. A microbalance, as shown in Fig. 1, is used to measure masses of 0–3 g with accuracy of 0.1 μg. Since these types of balances can be used everywhere, disturbing influences from the surrounding area can decrease the accuracy. Disturbing influences could be temperature changes, a draft of air, and floor vibrations [1].

To reduce the impact of floor vibrations, a vibration isolation system is used. In the last few years, research has been conducted on permanent-magnet-based levitation and isolation systems, e.g., in combination with mechanical [2]–[4] or fully magnetic [5]–[7] means, and in [8], the effects of errors in the magnetization direction on permanent-magnet-based systems are discussed. Such systems can be characterized by three important characteristics, i.e., force, stiffness, and resonance frequency. The key element in such a system is the magnetic spring. Since a magnetic spring is passively unstable, actuators or mechanical springs are also required to stabilize the system [9]. Compared with mechanical springs, permanent-magnet springs have the possibility of obtaining a high force output while maintaining low stiffness. This is advantageous since low stiffness is necessary to reject floor vibrations. Additional advantages are no mechanical wear, which results in lower maintenance costs and a high isolation bandwidth.

Manuscript received February 7, 2014; revised April 15, 2014; accepted April 30, 2014. Date of publication June 4, 2014; date of current version January 16, 2015. Paper 2014-EMC-0011.R1, presented at 2013 IEEE Energy Conversion Congress and Exposition, Denver, CO, USA, September 16–20, and approved for publication in the IEEE Transactions on Industry Applications by the Electric Machines Committee of the IEEE Industry Applications Society.

D. T. E. H. van Casteren and E. A. Lomonova are with the Electromechanics and Power Electronics Group, Department of Electrical Engineering, Eindhoven University of Technology, 5612 AZ Eindhoven, The Netherlands (e-mail: d.t.e.h.v.casteren@tue.nl; e.lomonova@tue.nl).

J. J. H. Paulides is with the Electromechanics and Power Electronics Group, Department of Electrical Engineering, Eindhoven University of Technology, 5612 AZ Eindhoven, The Netherlands, and also with AEGROUP, 5161 EA Sprang-Capelle, The Netherlands (e-mail: j.j.h.paulides@tue.nl).

J. L. G. Janssen is with Royal Philips, 5656 AE Eindhoven, The Netherlands (e-mail: j.l.g.janssen@tue.nl).

Color versions of one or more of the figures in this paper are available online at http://ieeexplore.ieee.org.

Digital Object Identifier 10.1109/TIA.2014.2328780

Fig. 1. Example of a microbalance [10].

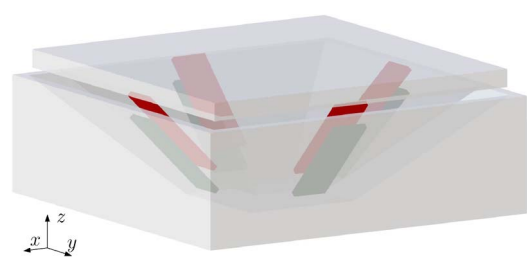

Fig. 2. Example of a cone-shaped vibration isolator.

In [11], a 3-D analytical magnetic surface charge model is used to calculate the suspension characteristics of several magnet topologies. In order to obtain low stiffness, positive and negative springs are combined. The considered magnet topologies are, however, only strictly horizontal or vertical. In [12] an angled, single-pole, gravity compensator was discussed. In this paper, the characteristics of a cone-shaped magnet topology, as shown in Fig. 2, are calculated to obtain the optimal angle of the cone.

II. Modeling Two Permanent Magnets

Using the analytical expressions discussed in [13]–[16], the force and stiffness can be calculated between two cuboidal permanent magnets. The expressions describe two magnetization combinations. For the first combination, both permanent magnets are magnetized along z. For the other combination, one

0093-9994 © 2014 IEEE. Personal use is permitted, but republication/redistribution requires IEEE permission.
See http://www.ieee.org/publications_standards/publications/rights/index.html for more information.

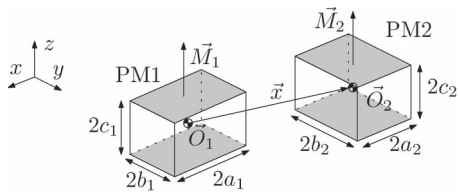

Fig. 3. Dimensions of two permanent magnets with parallel magnetization.

magnet is magnetized along z, and the other, along y. Hereafter, these combinations are referred to as parallel magnetization and perpendicular magnetization, respectively. All other combinations can be derived from these equations using superposition and coordinate rotation. In this paper, we will, however, only limit ourselves to parallel magnetization.

In Fig. 3, the dimensions of two parallel magnetized cuboidal magnets are shown. Both permanent magnets, i.e., PM1 and PM2, are studied in the Cartesian coordinate system. The dimensions of PM1 are given by $2a_1$, $2b_1$, and $2c_1$, and those of PM2 are given by $2a_2$, $2b_2$, and $2c_2$. The center of PM1, i.e., $\vec{O}_1$, is centered in the global coordinate system at $[0,\ 0,\ 0]^T$, and that of PM2, i.e., $\vec{O}_2$, is displaced by vector $\vec{x}$ given by $[\alpha,\ \beta,\ \gamma]^T$.

In the remainder of this section, the expressions derived in [13]–[16] are summarized.

A. Force Calculation

To calculate the force on PM2, the Lorentz force equation is used. The Lorentz force equation can be written as

$$\vec{F} = \int\int_S \sigma_{m_2} \vec{B}_1(\vec{x})\, ds \tag{1}$$

where σ_{m_2} represents the surface charge density of PM2, and $\vec{B}_1$ is the analytically obtained flux density from PM1. In the case of parallel magnetization, the resulting force equations have the following form:

$$\vec{F} = \frac{B_{r_1} B_{r_2}}{4\pi\mu_0} \sum_{i,j,k,l,m,n=0}^{1} (-1)^{i+j+k+l+m+n} \vec{\xi}(u,\ v,\ w). \tag{2}$$

In this equation, B_{r_1} and B_{r_2} are the respective remanent flux densities of the permanent magnets along the considered axes, i.e., $B_{r_1}\vec{e}_z$ and $B_{r_2}\vec{e}_z$, respectively. The intermediate variable $\vec{\xi}$ is an analytical function, which is given by

$$\begin{aligned}\xi_x &= \frac{1}{2}ur + \frac{1}{2}(w^2 - v^2)\log(r+u) \\ &\quad + wv\tan^{-1}\left(\frac{vu}{wr}\right) - vu\log(r+v) \end{aligned} \tag{3}$$

$$\begin{aligned}\xi_y &= \frac{1}{2}vr + \frac{1}{2}(w^2 - u^2)\log(r+v) \\ &\quad + wu\tan^{-1}\left(\frac{vu}{wr}\right) - vu\log(r+u) \end{aligned} \tag{4}$$

$$\begin{aligned}\xi_z &= -wr + uw\log(r+u) + vw\log(r+v) \\ &\quad + uv\tan^{-1}\left(\frac{uv}{wr}\right). \end{aligned} \tag{5}$$

The intermediate variables u, v, w, and r depend on the dimensions $(a,\ b,\ c)$ and displacement between the magnets (α, β, γ) as follows:

$$\begin{aligned} u &= \alpha - (-1)^i a_1 + (-1)^j a_2 \\ v &= \beta - (-1)^k b_1 + (-1)^l b_2 \\ w &= \gamma - (-1)^m c_1 + (-1)^n c_2, \\ r &= \sqrt{u^2 + v^2 + w^2}. \end{aligned} \tag{6}$$

B. Stiffness Calculations

Using the analytical equations of force, an analytical equation of the stiffness can be calculated. The stiffness matrix is given by a 3×3 Jacobian matrix, i.e., J, of force vector $\vec{F}$ and has a similar form as the force expression, i.e.,

$$\boldsymbol{K} = \frac{B_{r_1} B_{r_2}}{4\pi\mu_0} \sum_{i,j,k,l,m,n=0}^{1} (-1)^{i+j+k+l+m+n} \boldsymbol{\Xi}(u,\ v,\ w) \tag{7}$$

$$\boldsymbol{\Xi}(u,\ v,\ w) = -J\left(\vec{\xi}(u,\ v,\ w)\right) \tag{8}$$

where the intermediate variable $\boldsymbol{\Xi}$, after some simplifications due to the summation, is given by

$$\Xi_{xx} = v\log(r+v) - r \tag{9}$$

$$\Xi_{xy} = v\log(r+u) + u\log(r+v) - w\tan^{-1}\left(\frac{uv}{wr}\right) \tag{10}$$

$$\Xi_{xz} = -w\log(r+u) - v\tan^{-1}\left(\frac{uv}{wr}\right) \tag{11}$$

$$\Xi_{yx} = v\log(r+u) + u\log(r+v) - w\tan^{-1}\left(\frac{uv}{wr}\right) \tag{12}$$

$$\Xi_{yy} = u\log(r+u) - r \tag{13}$$

$$\Xi_{yz} = -w\log(r+v) - u\tan^{-1}\left(\frac{uv}{wr}\right) \tag{14}$$

$$\Xi_{zx} = -w\log(r+u) - v\tan^{-1}\left(\frac{uv}{wr}\right) \tag{15}$$

$$\Xi_{zy} = -w\log(r+v) - u\tan^{-1}\left(\frac{uv}{wr}\right) \tag{16}$$

$$\Xi_{zz} = -u\log(r+u) - v\log(r+v) + 2r. \tag{17}$$

C. Resonance Frequency

Using vertical force F_z and stiffness matrix $\boldsymbol{K}$, the resonance frequency matrix, i.e., $\boldsymbol{f_r}$, of the vibration isolator is calculated by

$$\boldsymbol{f_r} = \frac{\boldsymbol{\omega_r}}{2\pi} = \frac{1}{2\pi}\sqrt{\frac{\boldsymbol{K}}{m}} = \frac{1}{2\pi}\sqrt{\frac{\boldsymbol{K}g}{F_z}} \tag{18}$$

where the gravitational constant is denoted by g, and m is the mass of the isolated object.

III. Modeling Cone-Shaped Vibration Isolator

The vibration isolator consists of a translator and a stator part, where the translator is able to move in the xyz plane. To stabilize the system, an actuator is used. One option for this actuator is a square voice coil actuator, as described in [17] and [18]. A cross section of the cone-shaped vibration isolator researched in this paper is shown in Fig. 4 when the translator is in its original position ($x = 0$, $y = 0$, and $z = 0$). Similar to

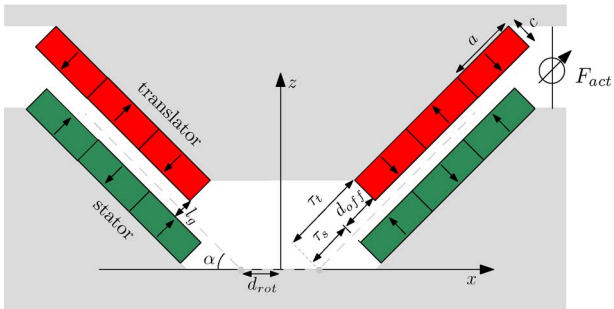

Fig. 4. Cross section of the investigated topology of the cone-shaped magnetic spring.

TABLE I
DIMENSIONS OF THE MAGNETS USED FOR MODELING THE CONE-SHAPED VIBRATION ISOLATOR

parameter	description	value
a	magnet length	$19.4{\cdot}10^{-3}$ m
b	magnet width	$20.0{\cdot}10^{-3}$ m
c	magnet thickness	$3.0{\cdot}10^{-3}$ m
B_r	magnet remanence	1.26 T
l_g	airgap length	$5.0{\cdot}10^{-3}$ m
μ_r	magnet permeability	1.00

the topologies in [11], the magnets are magnetized such that positive and negative springs are obtained. In this figure, only two of the four sides of the cone are shown. The actuator can be also used for active vibration isolation to achieve optimal isolation. This is, however, outside the scope of this paper.

In this paper, only the force, stiffness, and resonance frequency that occur during translations are treated. The rotations of the translator and the torque are outside the scope of this paper.

The dimensions $(a \times b \times c)$ of the magnets are the same for the translator and the stator. The air gap between the magnets is denoted by l_g. The magnets are rotated with an angle α around a point $d_{\rm rot}$ located from the origin. The distance between the rotation point and the stator or the translator is denoted by τ_s or τ_t, respectively, and the offset, i.e., $d_{\rm off}$, is the difference between τ_s and τ_t. The force generated by the actuators is denoted by $F_{\rm act}$.

To calculate the spring characteristics using the 3-D analytical magnetic surface charge model described in Section II, it is analytically determined that the distance between the sides is sufficiently large such that no magnetic interaction is present between the different sides of the cone. Using rotation and translation matrices, the combined force and stiffness of the four sides are calculated for various angles of the cone.

IV. RESULTS

Microbalances usually have a mass of about 10 kg; thus, the dimensions of the cone are chosen such that the output force is on the order of 100 N. The dimensions of the magnets used for modeling the vibration isolator are listed in Table I.

A. Experimental Validation

To validate the expressions derived in Section II, the results are not only compared with finite element (FE) results but also

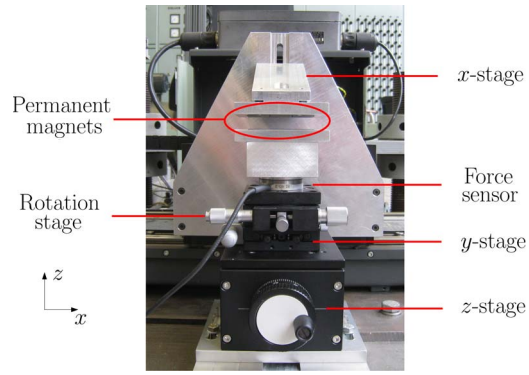

Fig. 5. Measurement setup with the ATI-MINI40-SI40-2 force sensor.

TABLE II
DIMENSIONS OF THE MAGNETS USED FOR THE MEASUREMENTS

parameter	description	value
a	magnet length	$19.25{\cdot}10^{-3}$ m
b	magnet width	$19.6{\cdot}10^{-3}$ m
c	magnet thickness	$3.06{\cdot}10^{-3}$ m
B_r	magnet remanence	0.9-1.26 T
l_g	airgap length	$5.3{\cdot}10^{-3}$ m
μ_r	magnet permeability	1.06

with experimental measurements. The setup of the measurement is shown in Fig. 5. The measurement is conducted for one side of the cone when the angle is zero. This is sufficient since the isolator consists of translated and rotated versions of the measurement, and these manipulations can be included in the model. The stator part is connected to a load cell, which is the ATI-MINI40-SI40-2 force and torque transducer. This sensor holds the stator part in a certain x and y position, whereas the translator part is moved along the y-direction by a linear drive.

The parameters of the magnets used during the measurements are listed in Table II. These parameters slightly vary from the parameters in Table I due to the available magnets. The magnets that are used have a relative permeability of 1.06. This is not taken into account by the analytical model, as described. Using the correction factor described in [19], the μ_r of a magnet can be modeled by adapting the B_r of the magnet with

$$B_r^{\rm new} = \frac{2B_r}{\mu_r + 1}. \tag{19}$$

In Table II, it is shown that there is a large deviation in the magnet remanence. This is because two of the six magnets were much weaker than the rest. These two magnets had $B_r = 0.9$, whereas the other four had a B_r of around 1.26.

In Fig. 6(a), the force is shown for the analytical model and the FE model, where $\mu_r = 1.06$, and for the measurements. The results show a high level of concordance between the analytical and FE results. However, when comparing the results with the measurements, small differences occur. These errors are shown in Fig. 6(b). It can be seen that the maximum error is about 10% of the maximum value of the force. The errors occur mainly due to the magnets in the setup. Since they are not ideal, there are several tolerances on their parameters. These tolerances in the magnet can be clearly seen in the shape of the force in the

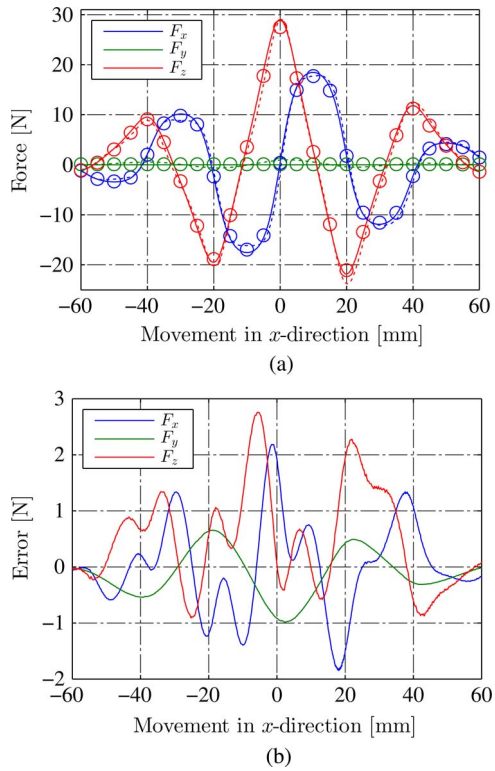

Fig. 6. (a) Resulting force in the x-, y-, and z-directions for the analytical model (solid), the FE model (o), and the measurement (dotted) for $\mu_r = 1.06$. (b) Error is given.

x-direction. In the case of the models, the shape is perfectly sinusoidal, whereas this is not the case for the measurement.

The tolerances consist of the following:

- the size variations of the magnet due to manufacturing tolerances;
- the chamfers at the edges of the magnets;
- the value of the μ_r and B_r of the magnet;
- the nonuniform magnetization and relative permeability.

When measuring the force, all these tolerances combine, causing a relatively large error. Furthermore, the setup itself is also the cause of some errors because of misalignments, for instance.

Although the measurements and the models are not an exact match, it is still possible to use the analytical models to obtain the optimal angle since the overall shape of the results is the same.

B. Optimal Angle

Since there are several variables that can influence the calculation of the optimal value, namely, the x, y, and z positions of the translator, the angle, and the offset, the dependence of the x and y positions and the offset are eliminated to increase the simplicity of the results. First, the dependence of the xy movement of the translator on the force and stiffness is discussed. Second, the optimal combination of the angle and the offset are combined. Finally, the optimal results for various movements in z are denoted.

1) xy Movement Dependence: In Figs. 7 and 8, the results of vertical force F_z and the vertical stiffness, i.e., K_{zz}, are

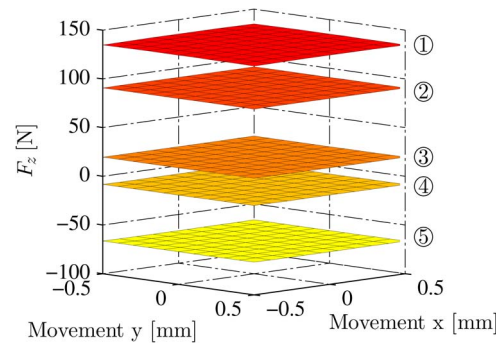

Fig. 7. Vertical force F_z for various combinations of the angle and the offset in the xy plane.

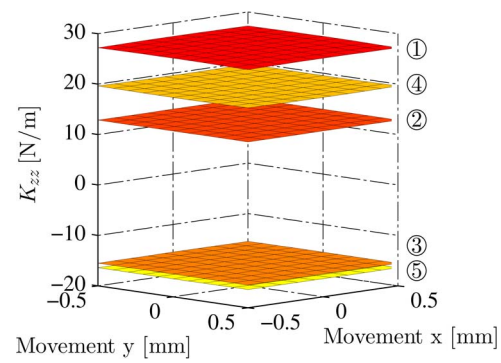

Fig. 8. Vertical stiffness K_{zz} for various combinations of the angle and the offset in the xy plane.

TABLE III
COMBINATIONS OF THE OFFSET AND THE ANGLE USED FOR THE RESULTS IN FIG. 7

Combination	Offset (mm)	Angle (°)
①	4	10
②	12	70
③	-4	50
④	-20	90
⑤	-12	30

shown for various arbitrary combinations of angle α and offset d_{off}, which are listed in Table III. These results are taken at a fixed z position. It can be seen that the vertical force and stiffness are flat surfaces. Therefore, it is possible to eliminate the xy position dependence by taking the mean value. This also holds for the horizontal stiffness, i.e., K_{xx} and K_{yy}.

Fig. 9 shows the mean value of the vertical force without z movement. It clearly shows that the maximal vertical force is achieved when the angle and the offset are both zero. Per angle, the maximal force is achieved at an offset, which increases when the angle increases, e.g., at 30°, the maximum is for an offset of 2.1 mm, and at 60°, the maximum is at an offset of 4.5 mm.

In Figs. 10 and 11, the mean values of the horizontal stiffness and the vertical stiffness, respectively, are shown. It can be seen that when the vertical force has its maximum value, the horizontal stiffness and the vertical stiffness have their maximal negative stiffness and maximal positive stiffness, respectively.

2) Ideal Combination: The ideal combination between the offset and the angle is chosen to be combinations where the vertical stiffness is zero. These points are indicated by the black

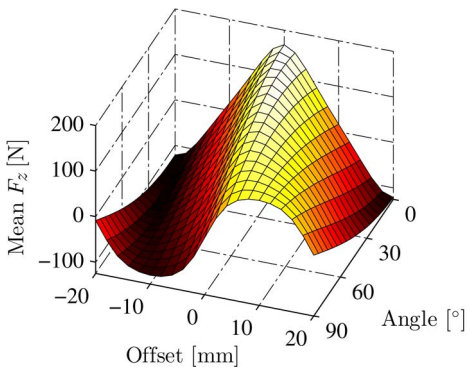

Fig. 9. Mean vertical force for different angles and offsets.

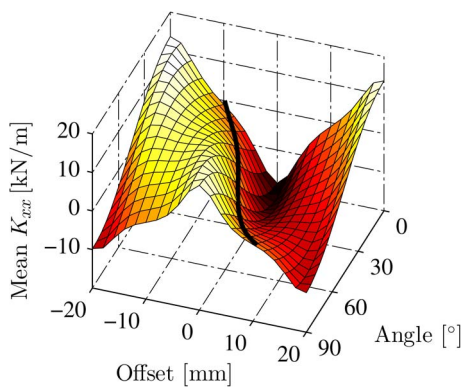

Fig. 10. Mean horizontal stiffness for different angles and offsets. The black line denotes the optimal combination between the angle and the offset.

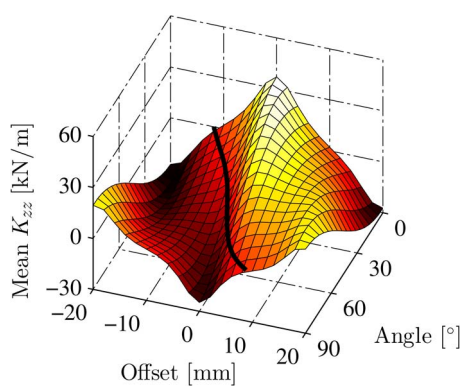

Fig. 11. Mean vertical stiffness for different angles and offset. The black line denotes the optimal combination between the angle and the offset.

line in Fig. 11. To see the resulting horizontal stiffness for these combinations, in Fig. 10, these combinations are also displayed as a black line. It can be seen that the horizontal stiffness is also zero for these combinations. Note that, due to the symmetry of the cone, it is only necessary to analyze the horizontal stiffness in the x-direction.

3) Optimal Results: During the preceding analysis, the initial z position, i.e., $z = 0$, was used to calculate the characteristics. However, the combinations of the angle and the offset allows to determine the optimal angle of the cone by deriving the mean of the horizontal stiffness and the vertical stiffness in the xy plane for different z positions. In Figs. 12 and 13, the mean horizontal stiffness and the mean vertical stiffness, respectively, are shown for different angles. Notice that both

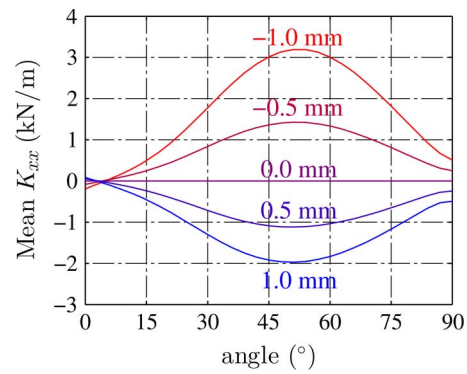

Fig. 12. Mean of horizontal stiffness K_{xx} for different z positions for a variation of angle α. The offset of the translator is chosen such that the stiffness for $z = 0$ mm is zero.

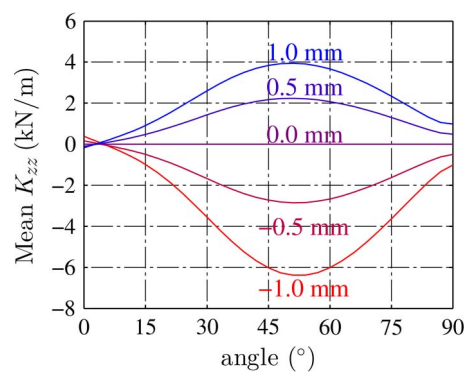

Fig. 13. Mean of vertical stiffness K_{zz} for different z positions for a variation of angle α. The offset of the translator is chosen such that the stiffness for $z = 0$ mm is zero.

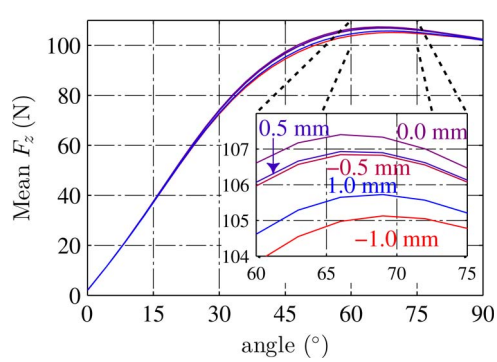

Fig. 14. Mean of vertical force F_z for different z positions for a variation of angle α. The offset of the translator is chosen such that the stiffness for $z = 0$ mm is zero.

the vertical stiffness and the horizontal stiffness for $z = 0$ equal zero. Furthermore, it can be seen that there are two optimal angles where the stiffness is minimal for all z positions, i.e., 4° and 90°.

As aforementioned, in addition to stiffness, other important characteristics of a magnetic spring are the vertical force and the resonance frequency and, therefore, should be also taken into account when determining the optimal angle. In Fig. 14, the mean vertical force for different angles is given for different z positions. It can be seen that the largest differences appear between an angle of 30° and 75°. This is due to the fact that the mean vertical stiffness is largest in this region. When looking at

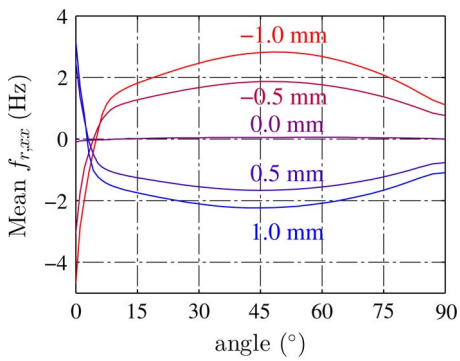

Fig. 15. Mean of horizontal resonance frequency $f_{r,\,xx}$ for different z positions for a variation of angle α. The offset of the translator is chosen such that the stiffness for $z = 0$ mm is zero.

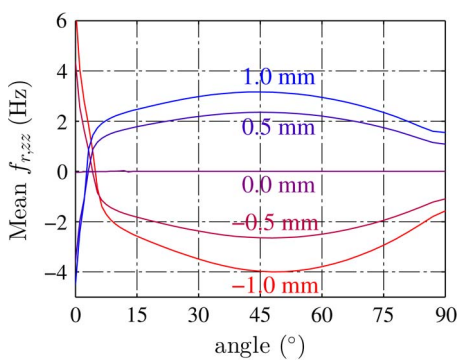

Fig. 16. Mean of vertical resonance frequency $f_{r,\,zz}$ for different z positions for a variation of angle α. The offset of the translator is chosen such that the stiffness for $z = 0$ mm is zero.

the optimal angles, a large difference in the vertical force can be seen. At an angle of 4°, the vertical force is 11 N, whereas at 90°, it is 102 N.

When calculating resonance frequency f_r using (18), imaginary resonance frequencies also occur due to the presence of negative stiffness. Although imaginary resonance frequencies are only theoretical, it still describes the relation between the stiffness and the force. Therefore, it is still useful for obtaining the optimal angle. To allow representation within the figures, imaginary values are plotted as negative resonance frequencies. In Figs. 15 and 16, the resulting mean horizontal and vertical resonance frequencies, i.e., $f_{r,\,xx}$ and $f_{r,\,zz}$, respectively, for different angles are given for different z positions. It is shown that the resonance frequency at 4° has a smaller absolute value than at 90° for different z positions.

Note that the optimal angle is dependent on the size of the magnets. For instance, when the magnets are $40 \times 40 \times 3$, the optimal angles are at 24° and 90°, and when the magnets are $30 \times 30 \times 3$, the optimal angles are at 16° and 90°. In Fig. 17, the optimal angles are given for various sizes of the magnets. It is shown that when a increases, the optimal angle increases, and when b increases, the optimal angle decreases. Furthermore, it can be seen that the optimal angle rapidly increases in the beginning with an increase in a, and then, it slows down.

Instead of changing the width of the magnets, the height of the magnets can be also varied. This is beneficial since in some cases, it might be important to reduce the weight of the levitated

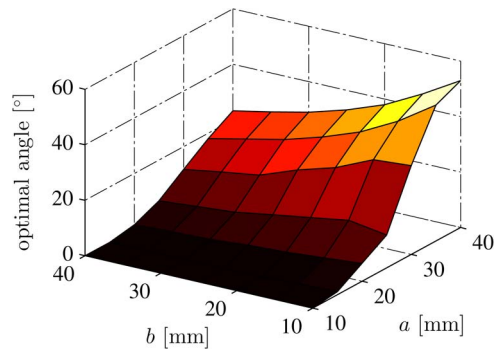

Fig. 17. Optimal angles for various sizes of the magnets.

TABLE IV
OPTIMAL ANGLE AND FORCE VALUES FOR SEVERAL HEIGHT VARIATIONS OF THE MAGNETS

c_1 [mm]	c_2 [mm]	optimal angle [°]	Force [N] @ angle	Force [N] max
3	1	5.3	4.9	43
	1.5	5.3	7.3	63
	3	3.7	10	107
	6	2.2	13	169
6	1	3.7	6.4	67
	1.7	3.2	9.6	107
	2	3.0	11	123
	3	2.2	13	169

mass. Reducing the height of the magnets on the levitated part will lead to less magnetic material, which results in weight loss and less magnetic force. To counteract the loss in the magnetic force, the height of the magnets on the stator can be enlarged. However, since the levitated mass is decreased, the magnetic force can be also smaller. This means less magnetic material, which decreases the costs of such a system.

To test the influence on the optimal angles and force characteristics, both the heights of the stator and translator magnets are independently varied using the magnets described in Table I. In Table IV, the results are shown. It can be seen that the optimal angle decreases when the height of the magnet increases. This also results in a larger force. When c_1 is doubled, as compared with the original magnets, c_2 should be 1.7 mm in order to obtain the same force characteristics. The optimal angle is, however, slightly lower.

V. CONCLUSION

In this paper, the spring characteristics of a cone-shaped vibration isolator for a microbalance have been discussed, and the optimal angle has been determined. Using a 3-D analytical model, the force, the stiffness, and the resonance frequency are calculated for various angles and offsets. When solely considering the stiffness, two angles, i.e., 4° and 90°, resulted in minimal stiffness variations for movements in z up to ±1 mm. The vertical force, however, was much lower for a 4° angle than for a 90° angle. The resulting mean resonance frequency showed the smallest variation in the case of a 4° angle.

To determine the optimal angle, the vibration isolators' volumetric envelope should be also considered. Since the vertical

force exerted by the magnets is nine times higher in the case of a 90° angle compared with the 4° angle, it will require much less space. Furthermore, in the case of a 90° angle, most volume is used in the vertical direction, whereas in the case of a 4° angle, more horizontal space is required. To conclude, without space limitations, 4° represents the optimal angle. However, when space is limited in the horizontal direction, it is better to use an angle of 90°.

Since the magnetic field of the isolator could influence the accuracy of the measurements, i.e., when a ferromagnetic material is weighted, more challenging research should be conducted on the shielding of magnetic fields of the vibration isolator. In addition, the influences of the temperature, presence of the actuator, and ferromagnetic material inside the scale should be researched.

REFERENCES

[1] *Proper Weighing With Laboratory Balances*, Mettler Toledo AG, Greiffense, Switzerland, May 2012.

[2] T. Mizuno, M. Takasaki, D. Kishita, and K. Hirakawa, "Vibration isolation system combining zero-power magnetic suspension with springs," *Control Eng. Pract.*, vol. 15, no. 2, pp. 187–196, Feb. 2007.

[3] M. E. Hoque, M. Takasaki, Y. Ishino, H. Suzuki, and T. Mizuno, "An active micro vibration isolator with zero-power controlled magnetic suspension technology," *JSME Int. J. Ser. C*, vol. 49, no. 3, pp. 719–726, 2006.

[4] D. T. E. H. van Casteren, B. L. J. Gysen, J. T. B. A. Kessels, J. J. H. Paulides, and E. A. Lomonova, "Non-linear full-car modeling and sky-hook control for a direct-drive active suspension system," *SAE Int. J. Passenger Cars, Mech. Syst.*, vol. 6, no. 1, pp. 252–268, Apr. 2013.

[5] J. L. G. Janssen, J. J. H. Paulides, and E. A. Lomonova, "Passive magnetic suspension limitations for gravity compensation," in *Proc. 11th ISMB*, Nara, Japan, Aug. 26–29, 2008, pp. 83–90.

[6] K. Nagaya and M. Ishikawa, "A noncontact permanent magnet levitation table with electromagnetic control and its vibration isolation method using direct disturbance cancellation combining optimal regulators," *IEEE Trans. Magn.*, vol. 31, no. 1, pp. 885–896, Jan. 1995.

[7] W. Robertson, B. Cazzolato, and A. Zander, "A multipole array magnetic spring," *IEEE Trans. Magn.*, vol. 41, no. 10, pp. 3826–3828, Oct. 2005.

[8] D. T. E. H. van Casteren, K. J. W. Pluk, J. J. H. Paulides, and E. A. Lomonova, "Modeling the effects of magnetization variations on a permanent magnet based levitation or vibration isolation system," in *Proc. LDIA Symp.*, 2013, pp. ID277-1–ID277-6.

[9] S. Earnshaw, "On the nature of the molecular forces which regulate the constitution of the luminuferous ether," *Trans. Camb. Philos. Soc.*, vol. 7, no. 1, pp. 97–112, 1839.

[10] *The First Class Choice For Valuable Samples*, Mettler Toledo AG, Greiffense, Switzerland, May 2008.

[11] J. L. G. Janssen, J. J. H. Paulides, and E. A. Lomonova, "Study of magnetic gravity compensator topologies using an abstraction in the analytical interaction equations," *Progr. Electromagn. Res.*, vol. 128, pp. 75–90, May 2012.

[12] W. Robertson, B. Cazzolato, and A. Zander, "Theoretical analysis of a non-contact spring with inclined permanent magnets for load-independent resonance frequency," *J. Sound Vib.*, vol. 331, no. 6, pp. 1331–1341, 2012.

[13] G. Akoun and J.-P. Yonnet, "3D analytical calculation of the forces exerted between two cuboidal magnets," *IEEE Trans. Magn.*, vol. MAG-20, no. 5, pp. 1962–1964, Sep. 1984.

[14] J. L. G. Janssen *et al.*, "Analytical calculation of interaction force between orthogonally magnetized permanent magnets," *Sensor Lett.*, vol. 7, no. 3, pp. 442–445, Jun. 2009.

[15] J. L. G. Janssen, J. J. H. Paulides, and E. A. Lomonova, "Analytical force and stiffness calculations for magnetic bearings and vibration isolation," in *Proc. ISEF*, Sep. 2009, pp. 1–8.

[16] H. Allag, J.-P. Yonnet, M. E. H. Latreche, and H. Bouchekara, "Coulombian model for 3D analytical calculation of the torque exerted on cuboidal permanent magnets with arbitrarily oriented polarizations," in *Proc. 8th Int. Conf. LDIA*, Jul. 2011, pp. 1–5.

[17] J. L. G. Janssen, J. J. H. Paulides, L. Encica, and E. A. Lomonova, "High-performance moving-coil actuators with double-sided PM arrays: A design comparison," in *Proc. ICEMS*, Incheon, Korea, Oct. 10–13, 2010, pp. 1603–1608.

[18] L. Encica, J. J. H. Paulides, D. Echeverria, E. A. Lomonova, and A. J. A. Vandenput, "A framework for efficient automated optimal design of electromagnetic actuators," in *Proc. 12th Biennial IEEE Conf. Electromagn. Field Comput.*, 2006, pp. 57–57.

[19] M. F. J. Kremers, J. J. H. Paulides, E. Ilhan, J. L. G. Janssen, and E. A. Lomonova, "Relative permeability in a 3D analytical surface charge model of permanent magnets," *IEEE Trans. Magn.*, vol. 49, no. 5, pp. 2299–2302, May 2013.

Dave T. E. H. van Casteren (S'13) was born in The Netherlands. He received the M.Sc. degree in electrical engineering from the Eindhoven University of Technology, Eindhoven, The Netherlands, where he is currently working toward the Ph.D. degree in the Electromechanics and Power Electronics Group, Department of Electrical Engineering.

His research is dedicated to permanent-magnet-based high-precision applications.

J. J. H. Paulides (M'03–SM'13) received the B.Eng. degree from Avans University of Applied Sciences, 's-Hertogenbosch, The Netherlands, in 1998 and the M.Phil. and Ph.D. degrees in electrical and electronic engineering from The University of Sheffield, Sheffield, U.K., in 2000 and 2005, respectively.

From 2005 to 2009, he held several postdoctoral positions with Eindhoven University of Technology, Eindhoven, The Netherlands, where he is currently a Part-Time Assistant Professor, focusing on more sustainable societies. He is also the Owner of AEGROUP, Sprang-Capelle, The Netherlands, which is a number of small- and medium-sized enterprises, which, among other activities, are prototyping and producing electrical machines. His research interests include all facets of electrical machines, particularly linear and rotating permanent-magnet excited machines for automotive and high-precision applications.

J. L. G. Janssen was born in Boxmeer, The Netherlands, in 1982. He received the M.Sc. and Ph.D. degrees in electrical engineering from the Eindhoven University of Technology, Eindhoven, The Netherlands, in 2006 and 2011, respectively. His research subject was electromagnetic vibration isolation, and in his project, he modeled, designed, and realized a high-performance vibration isolation system with permanent-magnet-based gravity compensation.

Currently, he is with Royal Philips, Eindhoven, The Netherlands.

E. A. Lomonova (M'04–SM'07) was born in Moscow, Russia. She received the M.Sc. (*cum laude*) and Ph.D. (*cum laude*) degrees in electromechanical engineering from the Moscow State Aviation Institute (TU), Moscow, Russia, in 1982 and 1993, respectively.

She is currently a Full Professor with and Chair of the Electromechanics and Power Electronics Group, Department of Electrical Engineering, Eindhoven University of Technology, Eindhoven, The Netherlands. She has worked on electromechanical actuators design, optimization, and development of advanced mechatronics systems.